Memory-Induced Chaos in Cardiac Excitation

Julian Landaw,[1,2] Alan Garfinkel,[1,3] James N. Weiss,[1,4] and Zhilin Qu[1,2,*]
[1]Department of Medicine (Cardiology), University of California, Los Angeles, California 90095, USA
[2]Department of Biomathematics, University of California, Los Angeles, California 90095, USA
[3]Department of Integrative Biology and Physiology, University of California, Los Angeles, California 90095, USA
[4]Department of Physiology, University of California, Los Angeles, California 90095, USA
(Received 8 August 2016; revised manuscript received 12 January 2017; published 28 March 2017)

Excitable systems display *memory*, but how memory affects the excitation dynamics of such systems remains to be elucidated. Here we use computer simulation of cardiac action potential models to demonstrate that memory can cause dynamical instabilities that result in complex excitation dynamics and chaos. We develop an iterated map model that correctly describes these dynamics and show that memory converts a monotonic first return map of action potential duration into a nonmonotonic one, resulting in a period-doubling bifurcation route to chaos.

DOI: 10.1103/PhysRevLett.118.138101

Memory has been widely studied not only in the brain [1], but also in many other systems [2–4] in physics, chemistry, and biology. When a system exhibits memory, its dynamical behavior depends on history, such as hysteresis in ferromagnets. In electrically excitable cells such as neurons and cardiomyocytes, the excitation dynamics are regulated by complex networks consisting of many types of ion channels and signaling pathways with multiple time scales, and therefore, these systems often exhibit short-term memory. For example, electrical bursting in neurons [5–8] and pancreatic β-cells [5] is caused by fast and slow time scales, and the slow time scales may give rise to short-term memory. In cardiac cells, the fast and slow time scales can give rise to early afterdepolarizations (EADs) that arise from the same Hopf-homoclinic bifurcation as in neurons and β-cells [9]. Complex electrical excitation dynamics are common in neural [10–13] and cardiac [14–21] cells, and low-dimensional iterated maps of action potential (AP) properties have been used to reveal the underlying mechanisms. These iterated maps do well when the memory effect is absent or small. However, in the presence of memory, low-dimensional maps may be insufficient, and higher-dimensional maps are usually needed to take into account the memory effects [22–24]. The effects of memory on cardiac alternans have been investigated in many previous studies [22–32], which generally have shown that memory suppresses alternans. In this study, we show that memory can potentiate dynamical instabilities to result in chaos and other complex excitation patterns in cardiac AP models, which can be well captured by an iterated map model that incorporates memory.

Simulations were carried out in a single cell with the equation of voltage (V) as

$$C_m \frac{dV}{dt} = -I_{\text{ion}} + I_{\text{sti}}, \tag{1}$$

where $C_m = 1\ \mu\text{F/cm}^2$ is the membrane capacitance, I_{ion} is the total ionic current density, and I_{sti} is the stimulus current density, which is a 0.5 ms square pulse of amplitude 80 $\mu\text{A/cm}^2$. $I_{\text{ion}} = I_{\text{Na}} + I_{si} + I_K + I_{K1} + I_{Kp} + I_b + I_{to,f}$, in which the formulations of the currents are from the 1991 Luo and Rudy (LR1) model [33] except that $I_{to,f} = g_{to,f} x_{to,f} y_{to,f} (V - E_K)$ is taken from the model by Mahajan *et al.* [34]. $I_{to,f}$ is the fast component of I_{to}, which activates and inactivates quickly. $g_{to,f}$ is the maximum conductance, and $x_{to,f}$ and $y_{to,f}$ are the activation and inactivation gating variables. The presence of I_{to} causes the so-called spike-and-dome morphology [Fig. 1(a)] and is associated with Brugada syndrome [35], a diseased condition with a high risk of sudden death. It has also been shown in previous simulation studies [36–39] and experiments [40] that I_{to} can promote alternans and complex AP duration (APD) dynamics, but the dynamical mechanisms remain to be elucidated, which are revealed in this study.

We calculated the S1S2 APD restitution curves in our simulations by pacing the cell periodically for several S1 beats and then applying an S2 beat with a certain S1S2 coupling interval [Fig. 1(b)]. Unlike the dynamic APD restitution used in many studies, the S1S2 APD restitution curve can be explicitly defined mathematically as

$$a_{n+1} = f(d_n), \tag{2}$$

where a_{n+1} is the APD of the S2 beat and d_n is the diastolic interval (DI) preceding the AP. For a periodically driven cell with period T, since $a_n + d_n = mT$ ($m = 1, 2, 3, \ldots$), Eq. (2) can be rewritten into an iterated map as

$$a_{n+1} = f(mT - a_n), \tag{3}$$

where mT is the actual excitation period. For example, $m = 1$ means every stimulus gives rise to an AP (1:1 capture), $m = 2$ means every two stimuli result in an AP

(2:1 failure), and so on. Equation (3) has been widely used to investigate APD dynamics under periodic stimulation [16–18,41–43].

Figure 1(c) shows S1S2 APD restitution curves for two S1 pacing periods in the original LR1 model in the absence of I_{to}. The APD restitution curve shifts slightly to the right for the shorter S1 pacing period, indicating that there is a very small memory effect. Figure 1(d) shows a bifurcation diagram of the LR1 model by plotting the APD against the pacing period T. 2:1 and 3:1 stimulation failure occurs, followed by chaos as T decreases. Chaos occurs only when T is very short (<100 ms). Figure 1(e) shows the bifurcation diagram obtained using Eq. (3) with the S1S2 APD restitution curve (black) in Fig. 1(c). The resulting bifurcation diagram is almost identical to the one from the LR1 model in Fig. 1(d), indicating that the S1S2 APD restitution curve combined with Eq. (3) can well describe the complex dynamics of the AP model.

We then added I_{to} to the LR1 model and changed several other parameters (see Fig. 1's legend). We shifted the steady-state curve of $y_{to,f}$ by 8 mV to more positive voltages. These changes were done to avoid nonmonotonic APD restitution curves and stimulation failure at fast pacing and thus to avoid the confounding effects of these properties on dynamical instabilities and chaos [43]. Adding I_{to} causes the APD restitution curve to be sigmoidal and sensitively depend on the S1 pacing period [Fig. 1(f)], indicative of a very large memory effect. The APD restitution curve shifts to the left for the shorter S1 pacing period, a different phenomenon from that in the original LR1 model [Fig. 1(c)] without I_{to}. Figure 1(g) shows a bifurcation diagram from the AP model using this parameter set, demonstrating a period-doubling route to chaos and an inverse period-doubling route to exit chaos as T decreases. Alternans and chaos occur at much slower pacing rates ($T \sim 900$ ms), and no stimulation failure occurs (APD is always shorter than T). In contrast, using Eq. (3) with the two APD restitution curves, the bifurcation diagrams exhibit only alternans [Fig. 1(h)] since the maximum slope of the APD restitution curve is greater than 1 [43]. This is because the APD restitution is a sigmoidal function. Therefore, without taking into account the memory effect, the simple iterated map based on the S1S2 APD restitution curve cannot capture the complex dynamics of the AP model, which is not surprising.

To analyze the mechanisms of the complex excitation dynamics induced by memory, we developed a new iterated map model that incorporates the memory effect. In the LR1 model, the slowly changing variable is the gating variable x of I_K, which recovers slowly during the DI phase [Fig. 2(a)]. Since in this model all other variables recover quickly after repolarization except x, we assume that the APD depends on the value of x at the beginning of the AP [labeled as x_n, Fig. 2(a)] as well as the DI, i.e.,

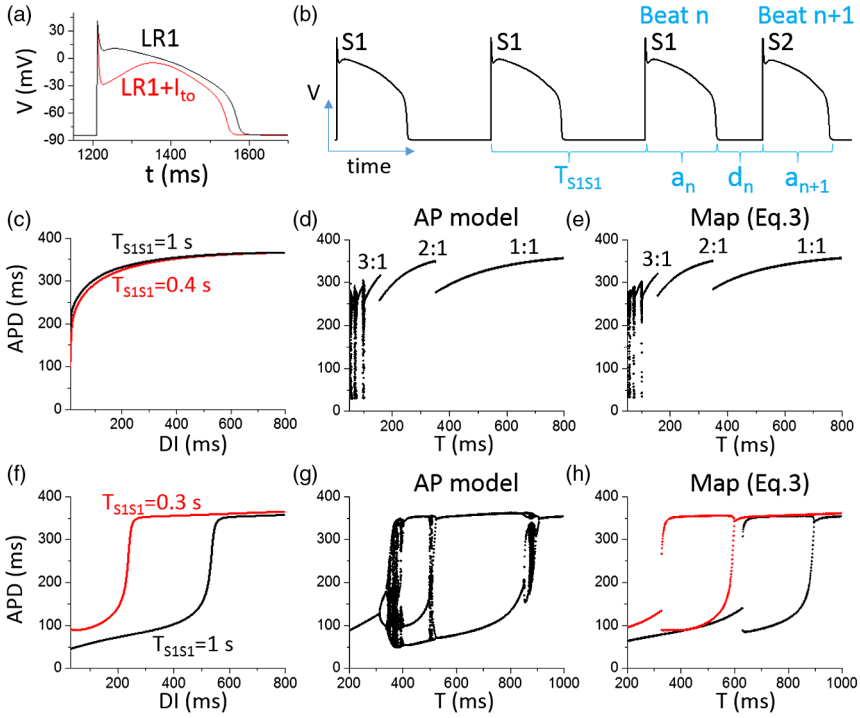

FIG. 1. (a) AP morphology change caused by I_{to}. (b) Voltage trace illustrating the S1S2 pacing protocol. (c) APD restitution curves of the original LR1 model for two S1 pacing periods (T_{S1S1}). (d) Bifurcation diagram (APD versus T) from the LR1 model. (e) Bifurcation diagrams using Eq. (3) and the APD restitution curves in (c). (f) APD restitution curves for two S1 pacing periods (T_{S1S1}) in the presence of I_{to} ($g_{to,f} = 0.21$ mS/cm^2). Other parameters changed from the original LR1 model are $G_{si} = 0.1035$ mS/cm^2, $G_{K1} = 1.33034$ mS/cm^2, and $\tau_x \to 5\tau_x$. The slope is greater than 1 between DI = 198 and 256 ms for the red curve and between DI = 495 and 555 ms for the black curve. (g) Bifurcation diagram of the AP model. (h) Bifurcation diagrams using Eq. (3) with the two APD restitution curves in (f), respectively.

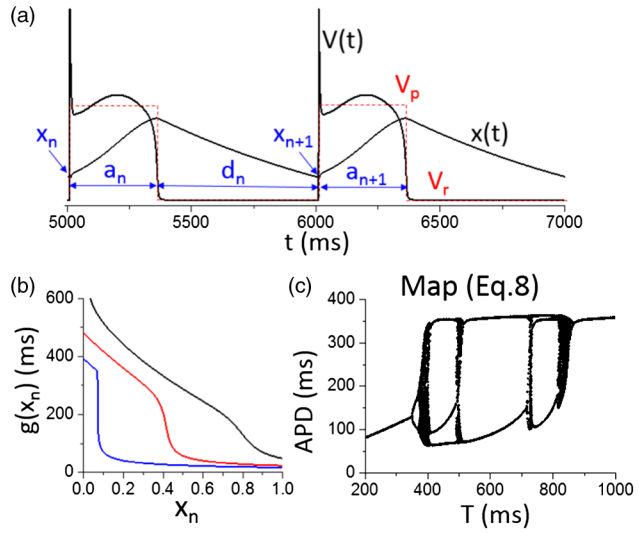

FIG. 2. (a) Black traces are V and x. The red dashed line is the voltage clamp trace for deriving Eq. (6). (b) The x-dependence curves of APD for $g_{to,f} = 0$ (black), 0.1 (red), 0.21 (blue), and 0.3 (green) mS/cm^2. DI = 500 ms. (c) Bifurcation diagram obtained using Eq. (8) [or Eqs. (6) and (7)] with the x-dependence curve of APD for $g_{to,f} = 0.21$ mS/cm^2 [the blue curve in (b)].

$$a_{n+1} = g(x_{n+1}, d_n), \tag{4}$$

in which we separate the APD dependence on the recovery of x and on the recovery of all other gating variables (lumped together in DI). To calculate the x-dependence of the APD in the LR1 model [i.e., function $g(x_n)$], after pacing for several beats we set different initial x values at the beginning of the AP (x_n) and measured the resulting APD (a_n). Figure 2(b) shows the APD dependence on x_n for different values of $g_{to,f}$ using a fixed DI = 500 ms. As $g_{to,f}$ increases, the x-dependence of APD becomes a steeper sigmoidal function and is left-shifted.

The next step is to derive an iterated map equation for x_n. In the AP model, the gating variable x is described by

$$\frac{dx}{dt} = [x_\infty(V) - x]/\tau_x(V). \tag{5}$$

Assuming a square voltage clamp [Fig. 2(a)] is applied to Eq. (5), one can solve Eq. (5) exactly to obtain the dependence of x_{n+1} on x_n as

$$x_{n+1} = [x_a - (x_a - x_n)e^{-(a_n/\tau_a)}]e^{-(d_n/\tau_d)} = w(x_n, a_n), \tag{6}$$

where we assume $x_\infty(V_r) = 0$ and define $x_\infty(V_p) = x_a$, $\tau_x(V_r) = \tau_d$, and $\tau_x(V_p) = \tau_a$. V_p is the constant voltage during the square pulse and V_r is the resting potential. In the original LR1 model, $x_a \sim 0.5$ for $V_p = 0$, $\tau_a \sim 600$ ms, and $\tau_d \sim 200$ ms. Since we made the parameter change $\tau_x \to 5\tau_x$, as in the simulation in Figs. 1(f)–1(h), we use $\tau_a = 3000$ ms and $\tau_d = 1000$ ms for the iterated map results shown in Figs. 2 and 3. As all other ionic currents recover quickly in the LR1 model, for simplicity, we ignore their contributions to restitution in the present study, and simply use

$$a_{n+1} = g(x_{n+1}). \tag{7}$$

From Eq. (7), we can express $x_n = g^{-1}(a_n)$. Inserting it into Eq. (6), we have $x_{n+1} = w[g^{-1}(a_n), a_n]$. Therefore, one can rewrite Eq. (7) into a first return map as

$$a_{n+1} = g\{w[g^{-1}(a_n), a_n]\} = G(a_n). \tag{8}$$

Using Eqs. (6) and (7) [or Eq. (8)] with the x-dependence curve of APD for the same $g_{to,f}$ as in Fig. 1(g), we obtained a bifurcation diagram [Fig. 2(c)] that is nearly identical to the one from the numerical simulation of the AP model [compare Fig. 2(c) with Fig. 1(g)]. Therefore, by adding memory into the iterated map model, one can accurately capture the complex excitation dynamics of the AP model, demonstrating that memory is key to the induction of the complex dynamics, including chaos.

To further theoretically analyze the mechanism of memory-induced chaos, we used a Hill function for g in Eq. (7) as

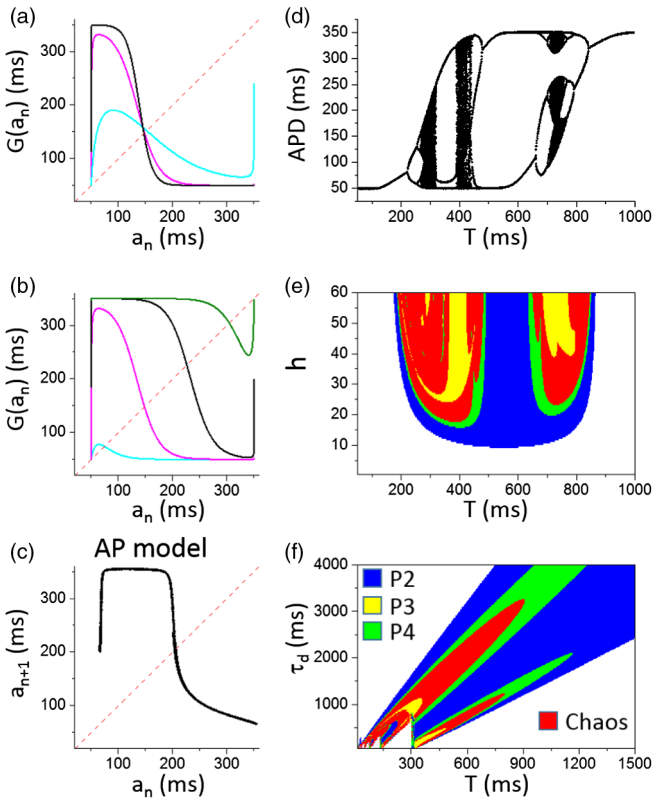

FIG. 3. (a) G versus a_n for $h = 40$ (black), 25 (magenta), and 10 (cyan). $T = 400$ ms. (b) G versus a_n for $T = 200$ (cyan), 400 (magenta), 600 (black), and 800 (olive) ms. (c) A first return map of the AP model in a chaotic regime [obtained from a chaotic trace at $T = 508$ ms; see Fig. 1(g)]. (d) A bifurcation diagram for the default set of parameters. (e) Phase diagram in the h-T space. (f) Phase diagram in the τ_d-T space. Except for panel (c), results in all the panels were obtained using Eq. (8) with the theoretical function in Eq. (9). P2 = period-2, P3 = period-3, and P4 = period-4.

$$g(x_{n+1}) = a_{\min} + \frac{a_{\max} - a_{\min}}{1 + (\frac{x_{n+1}}{k_d})^h}, \quad (9)$$

where h is the Hill coefficient, and $a_{\min}$ and $a_{\max}$ are the minimum and maximum APDs, respectively. We choose the following default set of parameters for the iterated map simulations in Fig. 3: $h = 25$, $k_d = 0.07$, $a_{\max} = 350$ ms, and $a_{\min} = 50$ ms. From Eq. (9), we have $x_n = g^{-1}(a_n) = k_d \sqrt[h]{(a_{\max} - a_n)/(a_n - a_{\min})}$, and so $G(a_n)$ in Eq. (8) is an explicit function of a_n. In Figs. 3(a) and 3(b), we plot G as a function of a_n under different conditions. Differing from function f in Eq. (3), the function G in Eq. (8) is no longer a sigmoidal function but a nonmonotonic function. Increasing h steepens the slope of G at the fixed point, causing the fixed point to be unstable. For very fast pacing or slow pacing, the slope of G at the fixed point is reduced, indicating that the fixed point is unstable for a certain range of T. In Fig. 3(c) we show a first return map from the AP model in a chaotic regime, showing that the first return map is nonmonotonic, very similar to the theoretical first return map in Figs. 3(a) and 3(b). Figure 3(d) is a bifurcation diagram obtained using Eq. (8), showing a period-doubling bifurcation route to chaos and an inverse period-doubling route out of chaos, a similar bifurcation structure to Figs. 1(g) or 2(c). Figure 3(e) shows a phase diagram in h-T space showing that increasing h promotes instabilities and chaos. Figure 3(f) shows a phase diagram in τ_d-T space with a fixed τ_a, showing that increasing τ_d increases the unstable range of T and causes the instability to occur at very long T.

Memory-induced chaos is not limited to the LR1 model but a general phenomenon in cardiac excitation. We carried out simulations using the human ventricular cell model by ten Tusscher *et al.* [44]. The simulation results are shown in Supplemental Material Fig. S1 [45]. When the original I_{to} (both fast and slow) was removed from the model, no instabilities occurred. When the same I_{to} model used for the LR1 model above was added, chaos and complex APD dynamics occurred [Fig. S1(c)]. The first return map of APD [Fig. S1(d)] is similar to the first return map shown in Fig. 3(c), indicating the same mechanism of chaos. By further analysis, we found that unlike the LR1 model, the memory in the ten Tusscher *et al.* model is not caused by the recovery of potassium currents but rather by accumulation of intracellular ions. However, a simple iterated map like Eq. (6) is no longer feasible since, for example, sodium accumulation affects intracellular calcium, thus requiring a more complex iterated map model to accurately model the dynamics [46]. We are developing a detailed iterated map model that will incorporate the memory effect caused by ionic accumulation to unravel the underlying complex dynamics.

Short-term memory can also potentiate complex dynamics and chaos in the setting of long QT syndrome [47]. Long QT syndrome is a cardiac disease with a high risk of syncope and sudden death, caused by genetic mutations or drugs that either decrease outward currents or increase inward currents to prolong APD [47]. One of the consequences is the occurrence of early afterdepolarizations (EADs) in the AP [Fig. 4(a)], which can lead to complex excitation dynamics [9,48]. Figure 4(b) is a bifurcation diagram from a simulation of the AP model, showing complex excitation patterns and chaos as the pacing period T increases. We also calculated the S1S2 APD restitution curves for two different S1 pacing periods. The S1S2 APD restitution curves exhibit a staircase-type increase against DI [Fig. 4(c)], with each higher step corresponding to an extra EAD in the AP. Faster S1 pacing causes the APD restitution curve to shift to the right. The bifurcation diagram [Fig. 4(d)] obtained using Eq. (3) and the APD restitution curves shows a sudden transition to APD alternans, which completely misses the bifurcation sequence of the AP model. We then used the same method as before to measure the x-dependence curve of APD [Fig. 4(e)]. Using the new iterated map model Eq. (8) [or Eqs. (6) and (7)], the bifurcation diagram [Fig. 4(f)] shows almost exactly the same bifurcation sequence as in the AP model. Bifurcation diagrams in wider ranges of T show that the iterated map model Eq. (8) can still capture the bifurcation sequences of the AP model (Supplemental Material Fig. S2 [45]). These results indicate that memory plays an important role in generating the complex EAD-related excitation dynamics.

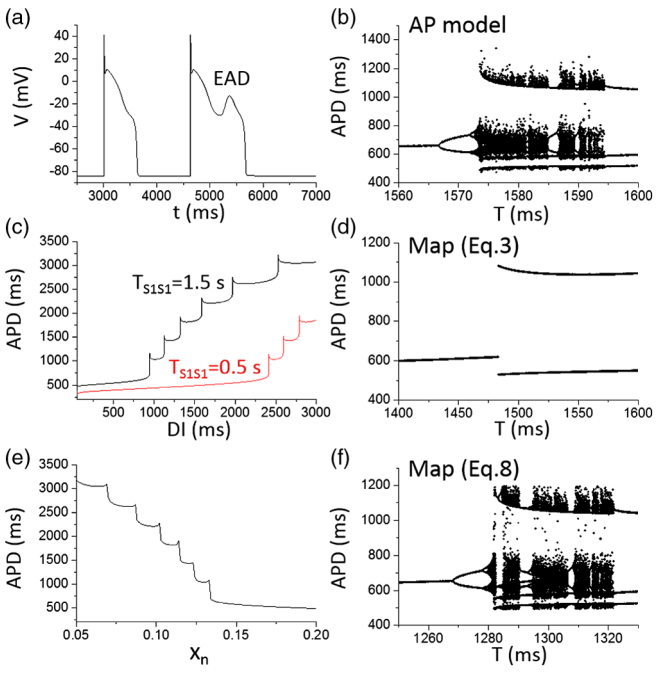

FIG. 4. (a) APs showing an EAD. All parameters are from the original LR1 model, except $\tau_x \to 10\tau_x$. (b) Bifurcation diagram from the LR1 model. (c) S1S2 APD restitution curves for two different S1 pacing periods (T_{S1S1}). (d) Bifurcation diagram obtained by iterating Eq. (3) with the S1S2 APD restitution curve (black) in (c). (e) APD versus x_n for DI = 1000 ms. (f) Bifurcation diagram obtained by iterating Eq. (8) [or Eqs. (6) and (7)] with the x-dependence curve of APD in (e).

In this study, we show that short-term memory can induce or potentiate complex excitation dynamics, including chaos, under certain cardiac disease conditions. The new iterated map model that incorporates memory properly can well describe the complex dynamics and unravel the underlying mechanisms, which may provide further understanding of memory and chaos in the genesis and maintenance of cardiac arrhythmias [48,49]. These mechanistic insights may not only be limited to complex excitation dynamics in cardiac myocytes but also to those in other electrically excitable cells. For example, the bursting dynamics in neurons [10–13] and pancreatic β-cells [5] are irregular, which can result from either random ion channel openings or dynamical chaos. Since the bursting dynamics are also governed by fast-slow dynamics [5–9] similar to the EAD dynamics in cardiac myocytes, the same mechanism of memory-induced chaos may be applicable to irregular bursting dynamics in these cases.

This study was supported by NIH Grant No. P01 HL078931 and by NIH training Grants No. T32 GM008185 and No. T32 GM008042.

*zqu@mednet.ucla.edu.

[1] E. R. Kandel, Science **294**, 1030 (2001).
[2] O. Auciello, J. F. Scott, and R. Ramesh, Phys. Today **51**, 22 (1998).
[3] K. N. Yugay, N. V. Blinov, and I. V. Shirokov, Phys. Rev. B **51**, 12737 (1995).
[4] W. Xiong and J. E. Ferrell, Jr., Nature (London) **426**, 460 (2003).
[5] J. P. Keener and J. Sneyd, *Mathematical Physiology* (Springer, New York, 1998), p. 766.
[6] C. A. Del Negro, C.-F. Hsiao, S. H. Chandler, and A. Garfinkel, Biophys. J. **75**, 174 (1998).
[7] E. M. Izhikevich, Int. J. Bifurcation Chaos Appl. Sci. Eng. **10**, 1171 (2000).
[8] A. Shilnikov, R. L. Calabrese, and G. Cymbalyuk, Phys. Rev. E **71**, 056214 (2005).
[9] D. X. Tran, D. Sato, A. Yochelis, J. N. Weiss, A. Garfinkel, and Z. Qu, Phys. Rev. Lett. **102**, 258103 (2009).
[10] J. Rinzel and G. B. Ermentrout, Methods Neuronal Modeling **2**, 251 (1998).
[11] M. I. Rabinovich and H. D. I. Abarbanel, Neuroscience (N.Y.) **87**, 5 (1998).
[12] A. L. Shilnikov and N. F. Rulkov, Int. J. Bifurcation Chaos Appl. Sci. Eng. **13**, 3325 (2003).
[13] S. Achuthan and C. C. Canavier, J. Neurosci. **29**, 5218 (2009).
[14] M. R. Guevara, L. Glass, and A. Shrier, Science **214**, 1350 (1981).
[15] L. Glass, M. R. Guevara, A. Shrier, and R. Perez, Physica D (Amsterdam) **7**, 89 (1983).
[16] D. R. Chialvo, R. F. Gilmour, and J. Jalife, Nature (London) **343**, 653 (1990).
[17] A. Vinet, D. R. Chialvo, D. C. Michaels, and J. Jalife, Circ. Res. **67**, 1510 (1990).
[18] M. Watanabe, N. F. Otani, and R. F. Gilmour, Circ. Res. **76**, 915 (1995).
[19] T. Krogh-Madsen and D. J. Christini, Annu. Rev. Biomed. Eng. **14**, 179 (2012).
[20] A. Karma, Annu. Rev. Condens. Matter Phys. **4**, 313 (2013).
[21] Z. Qu, G. Hu, A. Garfinkel, and J. N. Weiss, Phys. Rep. **543**, 61 (2014).
[22] N. F. Otani and R. F. Gilmour, J. Theor. Biol. **187**, 409 (1997).
[23] J. J. Fox, E. Bodenschatz, and R. F. Gilmour, Phys. Rev. Lett. **89**, 138101 (2002).
[24] S. S. Kalb, E. G. Tolkacheva, D. G. Schaeffer, D. J. Gauthier, and W. Krassowska, Chaos **15**, 023701 (2005).
[25] E. G. Tolkacheva, D. G. Schaeffer, D. J. Gauthier, and W. Krassowska, Phys. Rev. E **67**, 031904 (2003).
[26] J. J. Fox, M. L Riccio, P. Drury, A. Werthman, and R. F Gilmour, New J. Phys. **5**, 101 (2003).
[27] E. G. Tolkacheva, M. M. Romeo, M. Guerraty, and D. J. Gauthier, Phys. Rev. E **69**, 031904 (2004).
[28] E. M. Cherry and F. H. Fenton, Am. J. Physiol. Heart. Circ. Physiol. **286**, H2332 (2004).
[29] A. Baher, Z. Qu, A. Hayatdavoudi, S. T. Lamp, M.-J. Yang, F. Xie, S. Turner, A. Garfinkel, and J. N. Weiss, Am. J. Physiol. Heart. Circ. Physiol. **292**, H180 (2007).
[30] A. Gizzi, E. M. Cherry, R. F. Gilmour, S. Luther, S. Filippi, and F. H. Fenton, Front. Physiol. **4**, 71 (2013).
[31] S. Mironov, J. Jalife, and E. G. Tolkacheva, Circulation **118**, 17 (2008).
[32] N. Wei, Y. Mori, and E. G. Tolkacheva, J. Theor. Biol. **367**, 21 (2015).
[33] C. H. Luo and Y. Rudy, Circ. Res. **68**, 1501 (1991).
[34] A. Mahajan *et al.*, Biophys. J. **94**, 392 (2008).
[35] C. Antzelevitch and G.-X. Yan, Heart Rhythm **12**, 1852 (2015).
[36] B. Hopenfeld, Heart Rhythm **3**, 345 (2006).
[37] Z. Qu, F. Xie, A. Garfinkel, J. N. Weiss, Front. Physiol. **1**, 154 (2010).
[38] A. Maoz, T. Krogh-Madsen, and D. J. Christini, Heart Rhythm **6**, 813 (2009).
[39] A. Maoz, D. J. Christini, and T. Krogh-Madsen, Europace **16**, 458 (2014).
[40] A. Lukas and C. Antzelevitch, Circulation **88**, 2903 (1993).
[41] M. R. Guevara, G. Ward, A. Shrier, and L. Glass, IEEE Comp. Cardiol. **562**, 167 (1984).
[42] A. Karma, Chaos **4**, 461 (1994).
[43] Z. Qu, Y. Shiferaw, and J. N. Weiss, Phys. Rev. E **75**, 011927 (2007).
[44] K. H. ten Tusscher, D. Noble, P. J. Noble, and A. V. Panfilov, Am. J. Physiol. Heart. Circ. Physiol. **286**, H1573 (2004).
[45] See Supplemental Material at http://link.aps.org/supplemental/10.1103/PhysRevLett.118.138101, for simulation results of the ten Tusscher model and more detailed results in the presence of EADs.
[46] Z. Qu, M. B. Liu, and M. Nivala, Sci. Rep. **6**, 35625 (2016).
[47] D. M. Roden, J. Int. Med. **259**, 59 (2006).
[48] D. Sato, L.-H. Xie, A. A. Sovari, D. X. Tran, N. Morita, F. Xie, H. Karagueuzian, A. Garfinkel, J. N. Weiss, and Z. Qu, Proc. Natl. Acad. Sci. U.S.A. **106**, 2983 (2009).
[49] Z. Qu, Prog. Biophys. Mol. Biol. **105**, 247 (2011).